

## Air-coupled ultrasonic tomography of solids: 2 Application to concrete elements

Kerry S. Hall\*<sup>1</sup> and John S. Popovics<sup>2a</sup>

<sup>1</sup>Department of Engineering, University of Southern Indiana, 8600 University Blvd, Evansville, IN 47712, USA

<sup>2</sup>Department of Civil and Environmental Engineering, University of Illinois at Urbana-Champaign, 205 N Mathews Ave, Urbana, IL 61801, USA

(Received February 12, 2014, Revised September 19, 2014, Accepted October 29, 2014)

**Abstract.** Applications of ultrasonic tomography to concrete structures have been reported for many years. However, practical and effective application of this tool for nondestructive assessment of internal concrete condition is hampered by time consuming transducer coupling that limits the amount of ultrasonic data that can be collected. This research aims to deploy recent developments in air-coupled ultrasonic measurements of solids, described in Part 1 of this paper set, to concrete in order to image internal inclusions. Ultrasonic signals are collected from concrete samples using a fully air-coupled (contactless) test configuration. These air coupled data are compared to those collected using partial semi-contact and full-contact test configurations. Two samples are considered: a 150 mm diameter cylinder with an internal circular void and a prism with 300 mm x 300 mm square cross-section that contains internal damaged regions and embedded reinforcement. The heterogeneous nature of concrete material structure complicates the application and interpretation of ultrasonic measurements and imaging. Volumetric inclusions within the concrete specimens are identified in the constructed velocity tomograms, but wave scattering at internal interfaces of the concrete disrupts the images. This disruption reduces defect detection accuracy as compared with tomograms built up of data collected from homogeneous solid samples (PVC) that are described in Part 1 of this paper set. Semi-contact measurements provide some improvement in accuracy through higher signal-to-noise ratio while still allowing for reasonably rapid data collection.

**Keywords:** concrete; contactless; imaging; non-destructive testing ultrasound; UPV

---

### 1. Introduction

The potential for ultrasonic imaging to characterize internal condition of concrete structures has been recognized for some time (Buyukosturk 1998), and examples of ultrasonic tomography applied to concrete elements can be found in the literature. Recent developments in ultrasonic array hardware have enabled one-sided near surface imaging approaches, such as synthetic aperture focusing technique (SAFT), to locate steel reinforcing bar, voids and other defects (Schabowicz 2013, Hoegh 2012, Hoegh 2011). The depth of penetration of SAFT-based reconstruction methods is limited however, and furthermore it is difficult to image vertical or steeply dipping interfaces, or to interrogate regions that are shadowed behind near surface reflector

---

\*Corresponding author, Assistant Professor, E-mail: [khall@usi.edu](mailto:khall@usi.edu)

sets (Müller *et al.* 2012), for example closely spaced steel reinforcing bars in concrete. Efforts to employ ultrasonic imaging to cover the full cross-section or volume of an element, for example through tomographic re-construction, have been more limited. Full-volume measurements are necessary to investigate the interior of concrete columns and beams, especially when dense reinforcement near the surface masks deeper reflections with one-sided imaging methods. Full-volume ultrasonic measurements carried out in laboratory conditions can produce images with resolution useful for detection of internal defects have been reported, but rely on ultrasonic data collected by contact transducers. (Aggelis 2013, Chai *et al.* 2011, Schickert *et al.* 2005, Rens *et al.* 2000). Although these studies use reasonably large specimens, up to 400 mm thick, the data sets collected to accurately image the defects are large and would require an impractically long period of time to collect in the field. Several examples of full thickness ultrasonic imaging in field studies have been reported as well. Tomographic approaches have been used to reconstruct ultrasonic velocity data in concrete drilled shafts collected by the cross-hole sonic logging (CSL) procedure (Kase and Ross 2004). However CSL requires the embedment of four water filled tubes within the material among which the ultrasonic data are collected, which is not possible for most concrete structures. Results from external tests applied at the concrete surface have been reported, but with relatively few measurements for the volume imaged. For example Shiotani *et al.* (2009) used multiple low frequency P-wave velocity measurements generated by a mechanical impact (not ultrasonic) to build a velocity tomogram of a concrete dam structure to monitor repair action. However the inherent low frequency provided by the impact event, and the relatively low number of test points (15 test points on either side) leads to coarse image resolution (Aggelis *et al.* 2011), in this case on the order of 0.5 m. Ferraro *et al.* (2013) used ultrasonic P-wave velocity (UPV) imaging to assess the integrity of bridge piers before and after barge impacts, but were limited in their data collection because “manual collection of the UPV tomography data is a lengthy process.” Rens and Kim (2007) applied ultrasonic tomography to the Quebec Street Bridge project in Denver, Colorado. The element imaged was a 1.1 meter thick concrete pier cap. Due to practical limitations on data collection in the field, only 16 measurements were made between two faces of the pier cap. The tomogram produced from this very limited data set merely highlighted the two measurement paths that gave the lowest velocity readings. These results demonstrate the need for more efficient methods of collecting large sets of ultrasonic measurements for tomography of concrete structures.

Field application of powerful ultrasonic full-volume imaging methods will be enabled with fully contactless sensing. Air-coupled transducers provide a contactless interface between sensor and test materials, so measurements can be performed using arrays of transducers and automated positioning systems to greatly accelerate data collection. However, wave energy insertion loss (signal attenuation) is a significant challenge in the non-destructive evaluation of solid materials using air-coupled sensors. Furthermore, ultrasonic wave scattering from large-scale heterogeneities of concrete disrupts and obscures ultrasonic data. Even so, measurements such as UPV that are concerned only with the excited P-wave time of flight are still relatively simple, provided that the received excitation is distinguishable from the ambient noise. If sufficient amplitude can be transmitted, then air-coupled P-wave velocity measurements could be useful for tomographic imaging. Work by a few researchers has shown that through-measurements of concrete are possible using fully air-coupled ultrasound. Different means are used to overcome the insertion and scattering losses. Cetrangolo and Popovics (2010) utilized wavelet filtering of a narrow-band piezoelectric transducer with a matching layer. Pulse arrivals were successfully identified for time of flight measurements to map voids in a plate. Berriman *et al.* (2005) used CMUTs with pulse

compression to measure UPV for comparison with contact measurements. However; in each of these applications the specimens being measured were relatively thin.

In this paper, we report application of full-thickness ultrasonic tomography using air-coupled transducers to relatively large and realistic reinforced concrete samples. The contactless nature of the transducers allows us to collect many consistent and reliable data, and achieve better ray coverage of the cross-section than would be practical with conventional contact measurements in a field setting. We demonstrate that ultrasonic tomograms can be developed from such samples and the use of semicontact measurements provides a good balance of speed and accuracy.

## 2. Experimental setup

### 2.1 Testing hardware

A fully air-coupled transmission system was developed to measure the first arrivals using an automated process. An electrostatic transducer set (Senscomp 600) was used to transmit and receive short pulses with a central frequency of approximately 50 kHz. This ultrasonic frequency content provides a good balance between penetrating ability in highly scattering material and suitable axial and lateral resolution to define internal inclusions. The sensor set was fixed in direct alignment and the sample was placed in between them with a 30 mm air gap between sensor and sample. Fig. 1 (left) shows the raw signal transmitted through air. An oscilloscope digitized the signals with a sampling rate of 10 MHz. Each of these signals was collected with 1000 time averages to improve the signal-to-noise ratio (SNR). A triangular weighted moving average filter was applied to attenuate high frequency noise content without significantly distorting the initial arrival indication of the 50 kHz pulse signals. The first arrival indication of the pulse in the time signal is determined using an amplitude threshold. The amplitude of the threshold is set just above the noise level which is determined separately for each collection of signals on one cross-section. In order to collect signals with lower SNR while maintaining some of the speed of air-coupled measurements, a semi-contact testing configuration was also developed. Semi-contact measurements involve an air-coupled transducer on one side and a transducer in physical contact with the specimen on the other side. For these tests the Senscomp 600 transducer again was used as the transmitter, but PCB accelerometers were used to receive the ultrasonic pulses on the opposite face of the specimen. This semi-contact configuration provided signal amplitudes approximately 50 times greater than the fully contactless configuration for measurements through the concrete prism. A gel-coupled contact transducer configuration was also used for comparison. A set of 54 kHz piezoelectric contact transducers, and associated pulser receiver unit, were used. This equipment set satisfies the requirements in ASTM test standard C597 for ultrasonic measurements in concrete. Fig. 1 shows a comparison of the transmitted signals for the three sensor configurations. The signals collected by the contact measurements through the concrete prism were about 20 times higher in amplitude than the semi-contact measurements and 100 times larger than the non-contact measurements. The non-contact signal amplitude is so low, relative to those of the contact and semi-contact signals, that the p-wave arrival is not observed in Fig. 1 right. However, the arrival of this pulse can be extracted and detected with appropriate signal processing despite the very low signal amplitude.

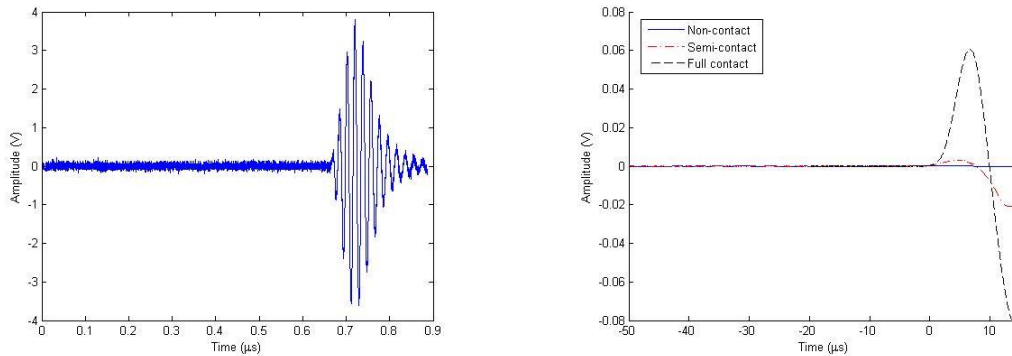


Fig. 1 Ultrasonic signal transmitted through air only (left) and ultrasonic signal showing early wave arrivals received through 305 mm concrete section using the three sensor configurations (right)

## 2.2 Specimens

For an initial test of contactless ultrasonic tomography for concrete sections, a 150 mm diameter cylindrical concrete specimen was cast with a cylindrical void 25 mm in diameter located 37 mm from the center of the cylinder. The void runs along the entire length of the cylinder. The concrete was composed of ASTM Type I cement with 15% replacement with silica fume, 10 mm limestone aggregate, and natural river sand. The mixture had a water/cement ratio of 0.35. These proportions were chosen in an attempt to simulate structural concrete containing coarse aggregates, while at the same time to have a material that will not promote excessive ultrasonic wave scattering, and thus have concrete that behaves closer to a homogeneous elastic solid in wave propagation tests. The latter issue is achieved by using a relatively small coarse aggregate and by minimizing the interfacial transition zone around the aggregates through the implementation of silica fume in the mixture.

In order to evaluate the practical application of ultrasonic tomography to realistic reinforced concrete elements, a separate mockup of a concrete column was constructed. A diagram of this specimen is provided in Fig. 2. The cross-section of the specimen was 305 mm by 305 mm square. The concrete for this specimen was composed of ASTM Type I cement with 25% replacement with class C flyash, 10 mm limestone aggregate, and natural river sand. The mixture had a water/cement ratio of 0.64 with a design strength of 35MPa at 90 days. These proportions were chosen to represent more conventional concrete.

In order to simulate damage within the column, 51 mm cubes of the same concrete mixture were cast in advance and loaded to just below their ultimate compressive strength. Care was taken to reverse the displacement of the load frame before the cubes were crushed completely which would result in a loss of shape. Four of these pre-crushed concrete cubes were carefully positioned and then cast into the column at two cross-sections, as shown in Fig. 2. These pre-crushed cubes act to simulate regions of localized cracking within the concrete element. In order to test for sensitivity of the tomograms to crack orientation, some of the cubes were placed with cracking oriented vertically (noted with a V in the figure) while others were placed with cracking oriented horizontally (noted with an H). The average P-wave velocity of the case where the wave

propagation path is perpendicular to the expected cracking direction was approximately 2230 m/s, which represents a reduction of 50% from the average P-wave velocity of undamaged concrete samples at the same age. In section A, two cubes were positioned near the center of the specimen at one elevation. In section B, the cubes were positioned near the corner of the specimen at another elevation. Two bars of 25 mm diameter deformed reinforcing steel were also embedded through the full length of the column to explore their effect on the tomographic imaging. In order to image these inclusions accurately, the pattern for collection of ultrasonic measurements through the prism was arranged carefully.

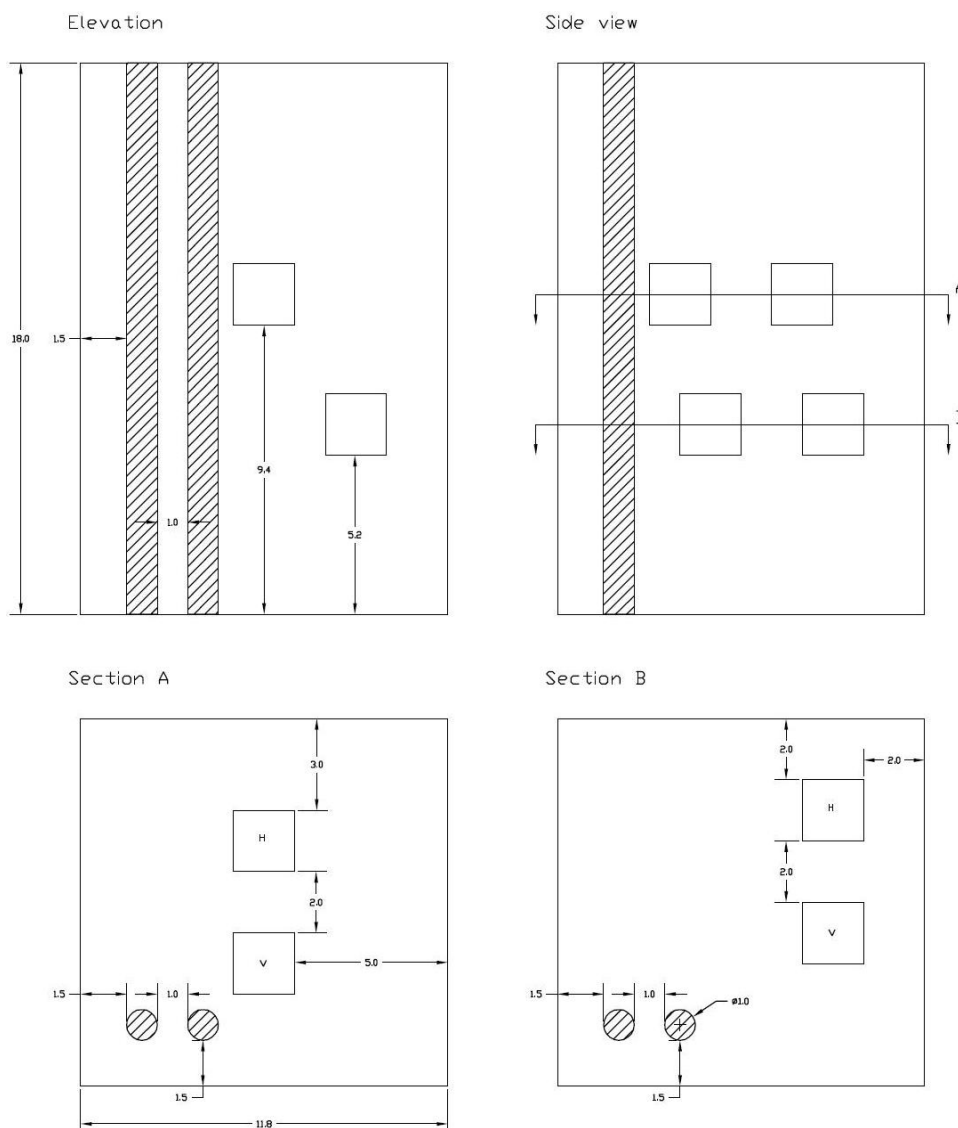


Fig. 2 Schematic of reinforcing bars and embedded damage cubes within square-section concrete specimen. All dimensions are in inches. Note: 1 inch = 25.4 mm

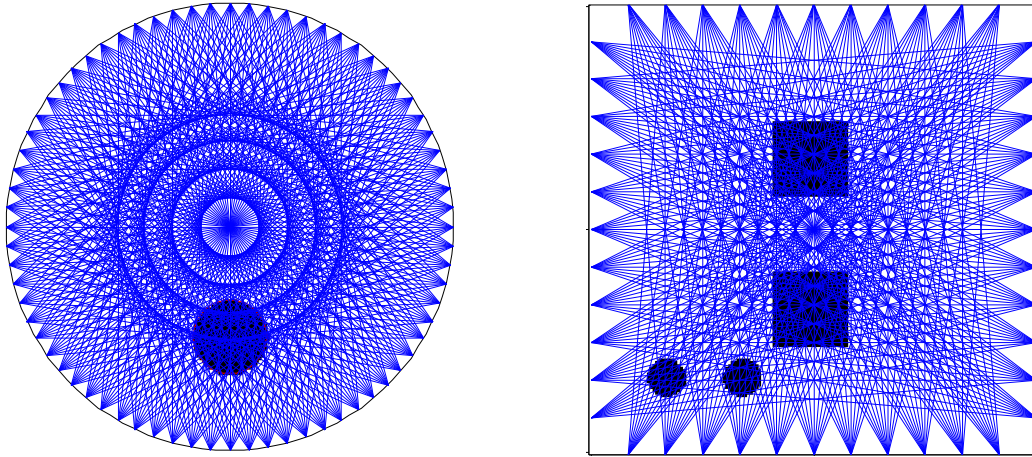


Fig. 3 Ray coverage diagram for the circular section (left) and for the square concrete section A with 25 mm transducer spacing (right). The black areas indicate the locations of inclusions

### 2.3 Measurement patterns (Ray Coverage)

The simulation study of Part 1 of this paper set (Hall and Popovics 2014) confirmed the importance of uniform ultrasonic ray distribution coverage over the entire area to be imaged, with rays intersecting throughout the specimen cross-section. For cylindrical specimens composed of uniform solid material, useful tomograms can be generated from appropriate air-coupled UPV measurements, where the tomograms indicate the location and extent of the internal inclusions with reasonable accuracy. In order to minimize error in tomograms for the general case, ray density and the fan width of ray angles should be maximized. In order to minimize error in tomograms for a specific sub-region in the sample, ray density and fan width of angles can be optimized.

For the concrete cylinder test, the sample was rotated at 5 degree increments to collect ultrasonic measurements in a cross-cutting network of ray paths throughout the sample. The data collection is repeated with the receiver in direct transmission as well as at offsets of 15, 30, and 45 degrees with respect to the center of the specimen. This results in relatively dense ray coverage that is distributed well over most of the area of the specimen as shown in Fig. 3.

The measurement pattern for the prism was chosen to follow the same principles. Ultrasonic waves were sent and received along multiple intersecting wave paths that lie on a single plane that is normal to the central axis of the prism. The transducer spacing was 25 mm across the surface of the specimen beginning 25 mm from the corner. For each transmitter position the receiver was positioned at each of the 11 receiver positions on the opposite face to collect one ultrasonic signal. Measurements were made only between transducers on opposite faces of the prism since measurements between adjacent faces resulted in lower amplitudes and distorted velocities. The direct transmission paths along the edges of the section were removed since these were anomalously slow. Fig. 3 shows the resulting ray coverage pattern. With 238 measurements over the entire cross-section at a variety of angles, this configuration provided good ray coverage for tomographic reconstruction. Ultrasonic measurements were collected using this same pattern by

three different test configurations: fully air-coupled, semi-contact with accelerometers on the receiving side, and conventional contact UPV.

## 2.4 Tomographic imaging

Tomographic inversion was performed using an algebraic reconstruction technique with a field of 30x30 pixels. The initial field was set to the average velocity of the material. After the tomogram is constructed, the field is interpolated bi-linearly for display. For more detailed information on the inversion and imaging process, refer to Hall (2011).

In order to compare tomograms quantitatively, an imaging error was calculated for each tomogram. Concrete naturally is an inhomogeneous and variable material, and this character is reflected in the measured wave velocity of the material. Thus we feel that analysis of absolute velocity cannot be used to characterize damaged or defected regions reliably. However relative changes in velocity, within a given inspection zone, may serve to identify such regions more reliably, assuming that appropriate relative velocity thresholds are set. In practice, a user of ultrasonic tomography on concrete must select a velocity threshold to identify inclusions that is specific to their test configuration and material characterization. In the reconstructed image, inclusion (void, cracks or rebar) areas were identified by pixels with velocity values within the lowest quarter of the complete velocity population in the tomogram. This 25% threshold was chosen after trial and error experimentation with various types of tomograms and testing configurations to accurately and consistently capture the location of defects. In practice, a user of ultrasonic tomography on concrete must select a velocity threshold to identify inclusions that is specific to each test configuration and material characterization.

Defect pixels (lowest quartile of velocity) were then assigned a value of 0, and pixels of solid material (remaining velocities) were assigned a value of 1. The image error was calculated as the difference between the location of predicted defects within a tomogram and the actual location prescribed defect in the finite element model, which is computed pixel by pixel. Data were collected from sections of the specimen with only rebar (without defects) for verification during the development of the method. Those results, which are not presented here, produced tomograms that indicated the location of the reinforcement, but with a significantly lower velocity than the remainder of the section. In these images, the 25% inclusion threshold gave around 1% error with respect to the location of the bars. Now for the case of section that contain defects, the pre-cracked cubes and bars account for 6.1% of the area of the square cross-section as shown in Fig. 2. So if a reduced spectrum tomogram indicates that 20% of the section is an inclusion, meaning that 20% of the pixels lie in the lower quartile of velocity, the error would be 13.9%. This quantification of error is useful for comparing tomograms in the experimental results of this work.

## 3. Experimental results

### 3.1 Fully contactless tomography of cylinder

The first concrete specimen to be imaged with fully contactless ultrasonic measurements was the cylinder with void inclusion. In Fig. 4 the dark regions indicate low velocity in the tomogram. The quality of the tomogram of the concrete cylinder is worse than those for homogeneous materials (c.f. ultrasonic tomograms of PVC specimens presented in Part 1 of this paper set).

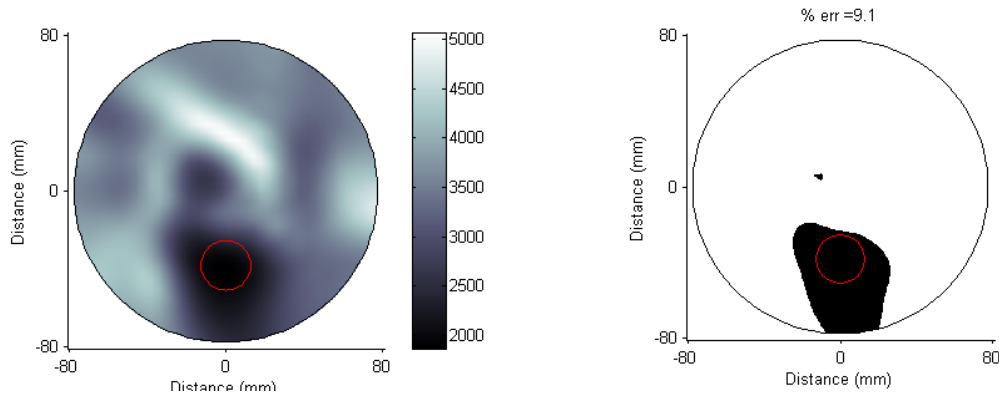


Fig. 4 Full velocity spectrum (left) and reduced spectrum (right) velocity tomograms of concrete-void specimen from fully contactless measurements. The units of velocity indicated by grayscale are meters per second. The red circle indicates the location of the void inclusions

Misalignment of the measurements is not likely the cause of the void distortion, since the same equipment and methods were used to collect the data. The relatively large acoustic impedance of concrete leads to a higher reflection coefficient at the interfaces with the air and reduces the received signal amplitudes, making it more difficult to accurately measure ultrasonic pulse velocity. Furthermore, the large-scale inhomogeneous nature of concrete causes ultrasonic wave scattering that attenuates and disperses the signals and adds noise, which reduces the SNR and adds variability to the UPV measurements. Nonetheless, there is still a clear indication of where the void is located within the specimen. This confirms that fully air coupled tomography of concrete is possible. The same methods were applied to the larger concrete prism to evaluate the feasibility of continued development for full scale application to concrete structures.

### 3.2 Fully contactless tomography of prism

Figs. 5 and 6 show the resulting tomograms from the reconstruction of the contactless air-coupled measurement sets for concrete prism along sections A and B, respectively. There are dark patches near the expected location of the cracking damage inclusions, but they are distorted and incorrectly located in both figures. There are also large false indications of low velocity inclusions. The reinforcement indications are also distorted and out of place. Although it is logical to expect that the steel reinforcement inclusion location should exhibit relatively higher velocity, they appear as low velocity zones in the tomograms using our experimental testing configuration. Our preliminary studies (not reported here) suggest that this is caused by the low SNR of the signal; the noise content obscures the arrival of the low amplitude wave transmitted through the higher velocity steel reinforcement. The UPV instead detects the larger amplitude signal of the wave traveling around the reinforcement, which indicates an apparent low velocity inclusion. The percent error of these tomograms (15-18%) is so high as to limit their usefulness in locating defects within concrete. The most troublesome errors are the dark areas that do not overlap the actual location of the inclusions. These errors are almost certainly the result of the very poor signal to noise ratio of fully air-coupled signals and greater attenuation through the larger cross-section.

The reduced SNR leads to inaccurate UPV measurements, which add false inclusion indications to the tomograms. In order to verify this, semi-contact measurements were employed with the same ray coverage pattern to image the same two cross-sections. Those results are presented in the next section.

### 3.3 Semi-contact tomography of prism

Figs. 7 and 8 show the resulting tomograms from the reconstruction of the semi-contact measurement sets. The semi-contact measurements were collected rapidly since multiple accelerometers could be deployed at once to receive simultaneous measurements. The errors in these tomograms (approximately 12%) are an improvement over the contactless measurements.

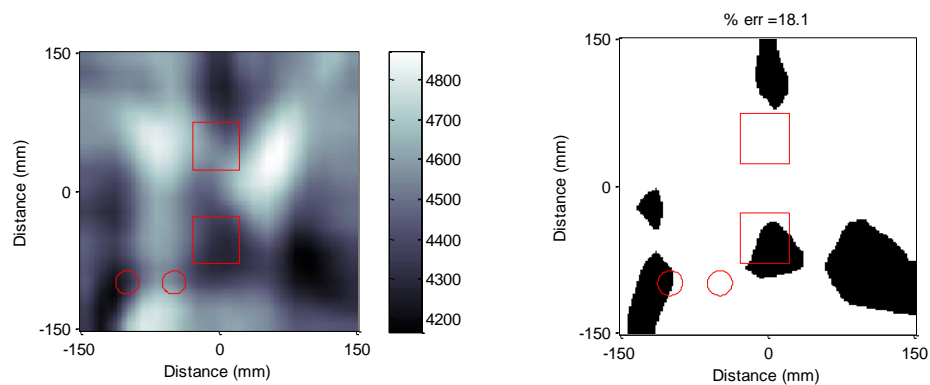


Fig. 5 Full velocity spectrum (left) and reduced spectrum (right) velocity tomograms of concrete with cracking section A from fully contactless measurements. The units of velocity indicated by grayscale are meters per second. The red lines indicate the locations of inclusions

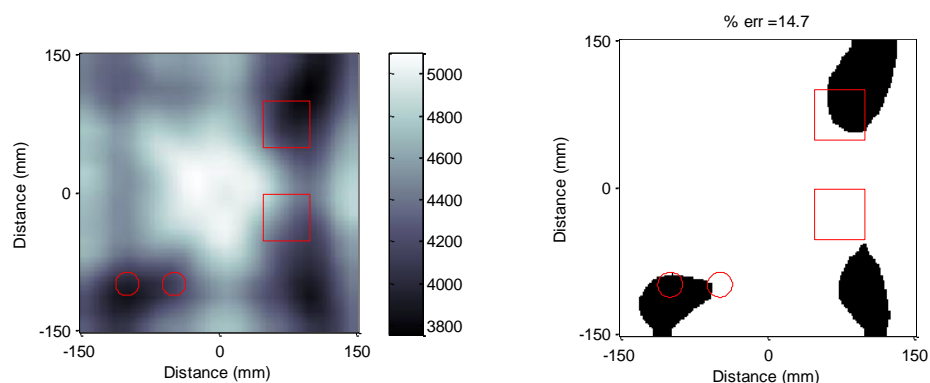


Fig. 6 Full velocity spectrum (left) and reduced spectrum (right) velocity tomograms of concrete with cracking section B from fully contactless measurements. The units of velocity indicated by grayscale are meters per second. The red lines indicate the locations of inclusions

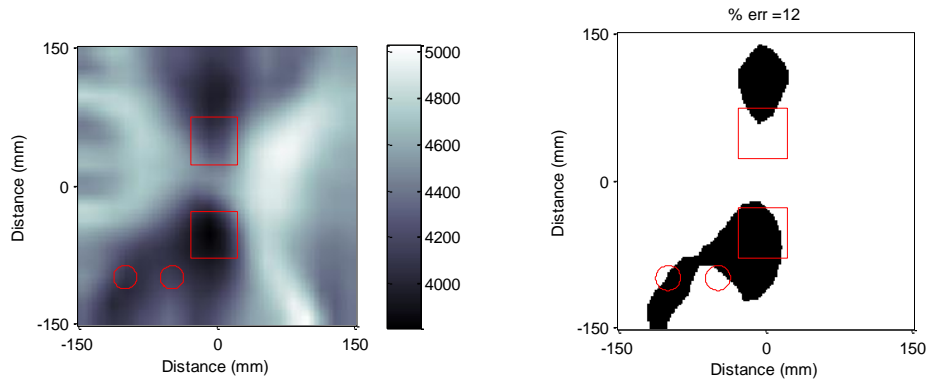


Fig. 7 Full velocity spectrum (left) and reduced spectrum (right) velocity tomograms of concrete with cracking section A from semi-contact measurements. The units of velocity indicated by grayscale are meters per second. The red lines indicate the locations of inclusions

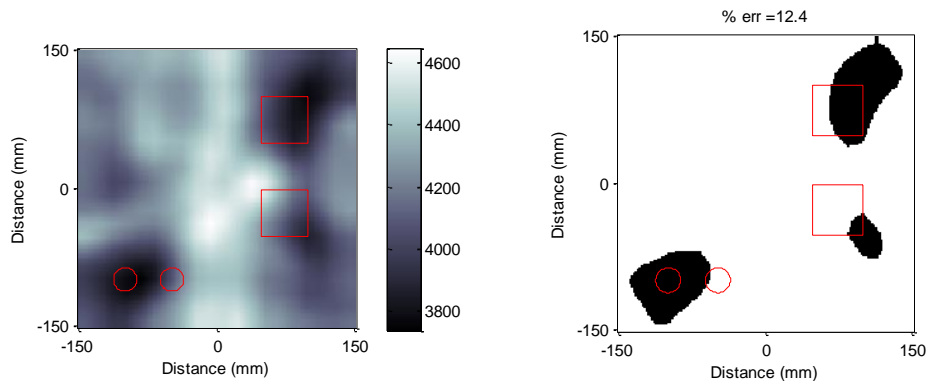


Fig. 8 Full velocity spectrum (left) and reduced spectrum (right) velocity tomograms of concrete with cracking section B from semi-contact measurements. The units of velocity indicated by grayscale are meters per second. The red lines indicate the locations of inclusions

The location of the damage inclusions is much better matched here and they are somewhat less distorted in both figures. The indications for the reinforcement are also closer to the actual positions of the bars. This gives more credibility that the low velocity indications are not simply artifacts in the images that happen to be near the actual inclusion locations. There are also fewer false low velocity indications. The increased accuracy can be attributed to the improved SNR of the semi-contact measurements. The accelerometers receive much greater amplitudes than the air-coupled receivers, but the air-coupled transmitter would still allow an automated positioning system to drive the test. Seeking further improvement in accuracy, we continued by collecting conventional full contact UPV for a third set of tomograms on the same two sections. Those results are presented next.

### 3.4 Contact tomography of prism

Figs. 9 and 10 show the resulting tomograms from the reconstruction of the conventional full contact UPV measurement sets. These measurements took the longest to collect since each measurement was collected separately and the transducers needed to be recoupled to the surface manually each time. The error in these tomograms (10-12%) is the lowest of the experimental data sets for these cross-sections as expected, but only slightly lower than the semi-contact data set. The indications of the damage areas in both figures are still distorted and slightly out of place. There are also still a few small false low velocity indications. The steel bar indications are much smaller in the full contact tomograms than in the images from the other two measurement sets. The reduced indication for the reinforcement might be due to the greater size of the transducers. Because the contact transducers average displacements from a larger surface area, they might be less sensitive to smaller inclusions.

Although the full contact signals are much higher in amplitude than the semi-contact signals, the quality of the reconstructions improve only slightly. The amplitude of the signals is an order of magnitude greater with the contact measurements, but the associated SNR increase is more modest because SNR is obtained on a logarithmic scale. Furthermore, the determination of arrival times remains uncertain, even for high amplitude signals obtained with a full contact configuration. Another factor contributing to error in the contact measurements is variability in the pressure manually applied and the quantity of couplant during coupling of the transducers to the concrete. The semi-contact measurements have more consistent coupling which may lead to more reliable P-wave velocity measurements.

While the full contact measurements resulted in the most accurate tomograms, the semi-contact measurements were not far behind in accuracy and provide great opportunity for much more rapid and consistent signal collection with the implementation of transducer arrays. With continued development of the data collection and analysis, semi-contact or contactless measurements could produce tomograms with better accuracy. The incorporation of bent ray analysis might improve the accuracy of velocity tomograms of concrete since the contrast in acoustic impedances is so high.

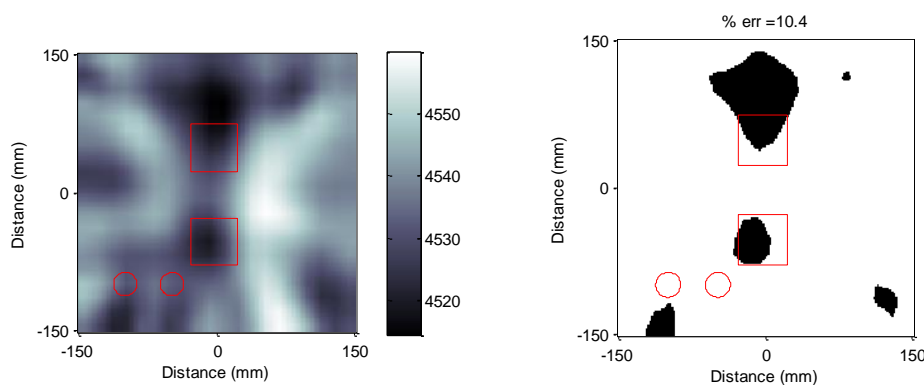


Fig. 9 Full velocity spectrum (left) and reduced spectrum (right) velocity tomograms of concrete with cracking section A from contact UPV measurements. The units of velocity indicated by grayscale are meters per second. The red lines indicate the locations of inclusions

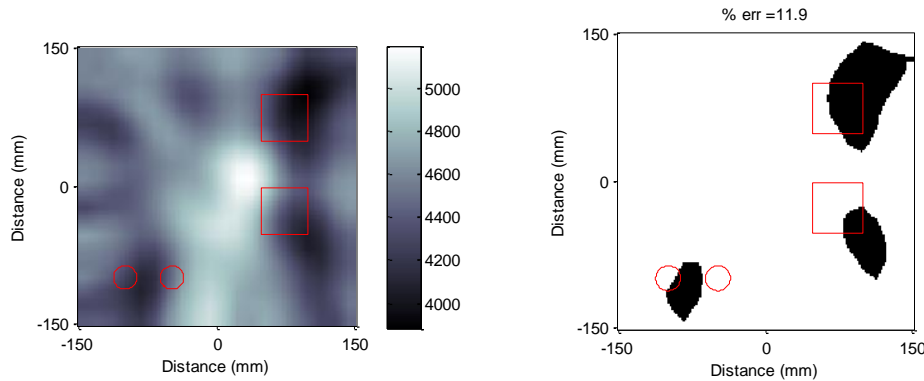


Fig. 10 Full velocity spectrum (left) and reduced spectrum (right) velocity tomograms of concrete with cracking section B from contact UPV measurements. The units of velocity indicated by grayscale are meters per second. The red lines indicate the locations of inclusions

The use of amplitude rather than velocity tomography might improve the images, or a hybrid velocity and amplitude tomogram might reduce noise. The authors are currently studying these topics in an ongoing research study.

#### 4. Conclusions

The following conclusions are drawn based on the results presented in this paper:

- Through thickness ultrasonic velocity tomograms that indicate the presence of different types of internal inclusions can be generated for conventional concrete samples using fully air-coupled ultrasonic measurements. However the quality of the images is lower than desired, as the position and size of the inclusions do exhibit some error.
- Tomograms built up with data from semi-coupled testing configurations show some improved accuracy with regard to inclusion position and size, brought by improved signal-to-noise ratio of the data.
- Tomograms built up with data from semi-coupled testing configurations are comparable to those built up with conventional contact ultrasonic measurements. Thus semi-coupled testing configurations offer a balance of image accuracy and time/labor efficiency.
- The inaccuracy in the ultrasonic images is mostly caused by the large-scale inhomogeneous nature of the concrete material, rather than the contact nature of the sensing.

The results presented in this paper demonstrate significant potential of contactless and semi-contact ultrasonic tests for through-thickness imaging of concrete elements. With continued development to the approach, for example though improved signal-to-noise ratio of the data and interpretation to account for material inhomogeneity, we expect that application to full scale concrete members will be practical and successful.

## Acknowledgments

This work carried out in the course of research funded by the National Science Foundation through NSF project CMMI 0710777, Dr. Lawrence C. Bank program manager. The authors would like to thank Dr. Gonzalo Gallo, Dr. Michael Oelze and Dr. Marc Goueygou for their helpful suggestions concerning this work.

## References

- Aggelis, D.G. (2013), "Wave propagation through engineering materials; assessment and monitoring of structures through non-destructive techniques", *Mater. Struct.*, **46**(4), 519-532.
- Aggelis, D.G., Tsimpris, N., Chai, H.K., Shiotani, T. and Kobayashi, Y. (2011), "Numerical simulation of elastic waves for visualization of defects", *Constr. Build.Mater.*, **25**(4), 1503-1512.
- ASTM Test Designation C 597-09 (2009), *Standard Test Method for Pulse Velocity through Concrete*, Annual Book of ASTM Standards, Vol. 04.02, West Conshohocken, PA
- Berriman, J., Purnell, P., Hutchins, D.A. and Neild, A. (2005), "Humidity and aggregate content correction factors for air-coupled ultrasonic evaluation of concrete", *Ultrasonics*, **43**(4), 211-217.
- Buyukosturk, O. (1998), "Imaging of concrete structures", *NDT&E Int.*, **31**(4), 233-243.
- Cetrangolo, G.P. and Popovics J.S. (2010), "Inspection of concrete using air-coupled ultrasonic pulse velocity", *ACI Mater. J.*, **107**(2), 155-163.
- Chai, H.K., Momoki, S., Kobayashi, Y., Aggelis, D.G. and Shiotani, T. (2011), "Tomographic reconstruction for concrete using attenuation of ultrasound", *NDT&E Int.*, **44**(2), 206-215.
- Ferraro, C.C., Boyd, A.J. and Consolazio, G.R. (2013), "Evaluation of damage to bridge piers using pulse velocity tomography", *Constr. Build. Mater.*, **38**, 1303-1309.
- Hall, K.S. and Popovics J.S. (2014), "Part1: Fully Air-Coupled Ultrasonic Tomography of Solids", *Smart Struct. Syst.*, Submitted (in review).
- Hall, K.S. (2011), *Air-coupled ultrasonic tomographic imaging of concrete elements*, Ph.D. Dissertation, University of Illinois Urbana-Champaign, Urbana, Illinois.
- Hoegh, K., Khazanovich, L. and Yu, H.T. (2012), "Concrete pavement joint diagnostics with ultrasonic tomography", *Transport. Res. Record*, **2305**, 54-61.
- Hoegh, K., Khazanovich, L. and Yu, H.T. (2011), "Ultrasonic tomography for evaluation of concrete pavements", *Transport. Res. Record*, **2232**, 85-94.
- Kase, E. and Ross T. (2004), "Seismic imaging as a means to evaluate foundation structures", in *Current Practices and Future in Deep Foundations*, Geotechnical Special Publication **125**, American Society for Civil Engineers, Reston, VA.
- Müller, S., Niederleithinger, E. and Bohlen T. (2012), "Reverse time migration: A seismic imaging technique applied to synthetic ultrasonic data", *Int. J. Geophys.*, **128465**.
- Rens, K.L. and Kim, T. (2007), "Inspection of Quebec street bridge in Denver, Colorado: Destructive and nondestructive testing", *J. Perform. Constr. Fac.*, **21**(3), 215-224.
- Rens, K.L., Transue, D.J. and Schuller. M.P. (2000), "Acoustic tomographic imaging of concrete infrastructure", *J. Infrastruct. Syst.*, **6**(1), 15-23.
- Schabowicz, K. (2013), "Ultrasonic tomography – The latest nondestructive technique for testing concrete members – Description, test methodology,application example", *Arch. Civil Mech. Eng.*, **14**(2), 295-303.
- Schickert, M. (2005), "Progress in ultrasonic imaging of concrete", *Mater. Struct.*, **38**(9), 807-815.
- Shiotani, T, Momoki, S., Chai, H.K. and Aggelis, D.G. (2009), "Elastic wave validation of large concrete structures repaired by means of cement grouting", *Constr. Build. Mater.*, **23**(7), 2647-2652.

